Case Report

Dabao Shi and Rui Zhang*

Long bone metastases of renal cell carcinoma imaging features: case report and literature review

https://doi.org/10.1515/oncologie-2023-0080
Received February 27, 2023; accepted May 14, 2023;
published online June 14, 2023

Abstract

Objectives: This article analyzed the imaging features of 18 long bone metastasis (LBM) of renal cell carcinoma (RCC) confirmed by pathology and reviewed the available literature.
Case presentation: Patients who underwent radiographic examinations at our hospital between January 2015 and December 2021 with pathology-confirmed bone metastases were evaluated. The clinical and radiographs and CT, and MR images features of the patients were analyzed. Eighteen patients with pathology-confirmed LBM from RCC were collected. All the patients had X-ray examinations, 15 had computed tomography (CT), 13 had magnetic resonance (MR) imaging, and six had MR enhancement. The clinical and imaging features of the lesions were analyzed, including morphological and signal intensity characteristics. Ten patients were found with metastases after nephrectomy, and eight patients were admitted to the hospital with skeletal-related events (SREs). Eighteen cases originated from clear cell RCC. Fourteen lesions were located in the epiphysis and four in the diaphysis. The height-to-width ratio of the lesions ranged from 1.11 to 3.41 (mean, 1.84). All lesions showed osteolytic destruction, with 16 lesions showing expansile destruction. Seven lesions demonstrated soap bubble hyperintensity and hypointense separation on T2-weighted images. Six lesions demonstrated a flow-void sign, and six showed marked marginal enhancement.
Conclusions: The LBM of RCC mainly occurred in the proximal epiphysis and tended to spread along the long bone axis with expansile osteolytic destruction. In some cases, soap bubble hyperintensity, hypointense separation, and the flow-void sign were seen.

Keywords: case report; long bone; metastasis; MR; renal cell carcinoma

Introduction

Renal cell carcinoma (RCC) is a clinically common malignant tumor worldwide. The major histologic subtype of RCC is clear cell RCC (ccRCC) [1–3]. ccRCC is prone to early hematogenous metastasis. Bone (20–40 %) is the second most common metastatic site of RCC after the lung (70 %) [2, 4, 5]. Although bone metastasis is far more prevalent than primary bone malignancy, solitary metastasis that occurs in the extremities is relatively rare. Solitary long bone metastasis (LBM) may accompany an occult primary renal tumor, or it may be delayed metastasis from a previously treated lesion [6]. Most of these patients are admitted to the hospital with bone pain and a pathological fracture as the first symptom. Therefore, imaging examination is of great significance for the early detection and diagnosis of LBM of RCC [5–9].

X-ray, computed tomography (CT), and magnetic resonance imaging (MRI) are the most common examination methods. Due to excellent soft tissue resolution, MRI is the preferred imaging modality of choice for assessing metastatic spread in the marrow cavity, an extension of the tumor from the marrow cavity, and the involvement of surrounding structures [8]. The sites of bone metastases from RCC have been reported, including the spine, ilium, skull, clavicle, rib, humerus, femur, tibia, and fibula [6, 10–15]. Fewer than 10 cases of solitary LBM were reported between 2000 and 2019 [5, 6, 13, 14]. The X-ray and CT images showed that the RCC metastases mostly had osteolytic destruction with expansile change, no periosteal reaction, and were soft-tissue masses [5, 12–15]. The MR images demonstrated hypervascularity, slight hypointensity or isointensity of the masses on T1-weighted images (T1WI), and hyperintensity or mixed signals on T2-weighted images

***Corresponding author: Rui Zhang**, Department of Radiology, Xiangyang Central Hospital, Affiliated Hospital of Hubei University of Arts and Science, Xiangyang, China, E-mail: skyzhangrui1992@163.com
Dabao Shi, Department of Radiology, Xiangyang Central Hospital, Affiliated Hospital of Hubei University of Arts and Science, Xiangyang, China

(T2WI) [6, 11, 13]. Salapura reported a case of a 71-year-old male patient with disseminated (including the right humerus) osteoblastic bone metastases from ccRCC [10].

The MR imaging of LBM of RCC might show certain characteristics. Two articles specifically reported the flow vessels of bone metastases from RCC [6, 7], but no articles have summarized the MR imaging features of a series of solitary LBMs. This article retrospectively analyzed the imaging features of 18 LBMs of RCC confirmed by pathology and reviewed the available literature, aiming to explore the imaging features and improve the accuracy of diagnosis.

Materials and methods

Patients

Patients who underwent radiographic examinations at our hospital between January 2015 and December 2021 with suspected bone metastases were evaluated. The inclusion criteria were: (1) long bone lesions pathologically confirmed as bone metastases of ccRCC and (2) patients with bone metastasis who underwent imaging examinations before the initiation of cancer-directed therapy. The clinical and imaging features of the patients were analyzed.

Imaging protocol

X-ray scanning was performed on a SIEMENS Ysio DR X-ray scanner. CT images were obtained using a multidetector CT scanner (Philips Brilliance, Philips Brilliance iCT, and Siemens Healthineers), with 64–256 detector rows. The sagittal and coronal images were reconstructed to obtain the axial images. The scanning parameters were 120 kV, automatic milliampere setting (range 80–320 mA), and a pitch of 1 and 5 mm contiguous section thickness. Imaging was followed by the use of bone tissue (window width (WW): 1,600–2,500 HU, window level (WL): 500–800 HU) and soft tissue (WW: 300–500 HU, WL: 45–60 HU) algorithms.

MR imaging was performed with a 3.0 T magnet (Siemens Medical Solutions, Germany). The imaging parameters were slightly different depending on the imaging site. The pre-contrast scanning sequences were axial T1WI (repetition time (TR)=500–520 ms, echo time (TE)=11–15 ms, 5 mm thickness); axial, coronal fat suppression T2WI (TR=3,500–4,000 ms, TE=81–138 ms, 5 mm thickness); and sagittal T2WI (TR=3,500–4,000 ms, TE=106–131 ms, 5 mm thickness). Enhanced scanning was performed by an intravenous injection of gadopentetate dimeglumine (Gd-DTPA, 3 mL/s, 0.1 mmol/kg), and the sequences also included axial, sagittal, and coronal enhanced T1WI scans (TR=160–185 ms, TE=1–2 ms, 5 mm thickness).

Image evaluation

Two experienced radiologists (with three and 10 years of work experience, respectively, in musculoskeletal imaging) separately reviewed all the images on a picture archiving and communication system. Any discordance was resolved by consensus. The morphological features of the lesions were evaluated on the radiographs and CT images, including the location (proximal epiphysis, diaphysis, and distal epiphysis), size (maximum height in the sagittal position and maximum width on axial view), height-to-width ratio (maximum height/maximum width), margins (well-defined or ill-defined), bone destruction (expansile or non-expansile), cortical bone (interruption or continuity), periosteal reaction, and soft-tissue mass.

The lesion signal intensity characteristics on MR images were analyzed, including the signal intensity of each sequence (lesion signal intensity lower than the signal intensity of muscle was described as hypointense; the same as the signal intensity of muscle, as isointense; greater than the signal intensity of muscle but less than the signal intensity of fat, as hyperintense), the signal uniformity on T2WI (uniformity or uneven), soap bubble sign (heterogeneous hyperintensity on T2WI), separation (curvilinear area of hypointensity in the mass on T2WI), flow-void sign (multiple dot-like or tubular structures with low signal intensity located within or around the lesion that probably corresponded to vessels) [6], enhancement amplitude (unenhanced, slightly enhanced, or markedly enhanced compared with surrounding normal enhancing muscle and vessels), and uniformity.

Case illustration

Clinical features

Eighteen patients (15 males, three females; age range, 48–74 years; average age, 63.8 ± 5.3 years) were included in this study. All patients had X-ray examinations, 15 had CT, 13 had MR imaging, and six had MR enhancement.

Metastases were found after nephrectomy in 10 patients, and the median time interval between nephrectomy and the diagnosis of metastasis was one year (range, 0.5 months–10 years). The other eight patients were admitted to the hospital with limb pain as the first symptom, and five patients progressed to pathological fractures, which were then diagnosed as having an RCC source. All of the ccRCCs were pathologically confirmed as well.

The mean follow-up period for 18 patients was 13.5 months (3–24 months). Nine patients underwent radiotherapy and chemotherapy, and another nine underwent surgery, followed by chemotherapy. During the follow-up period, 11 patients had multiple metastases in the axial skeleton, two had brain metastases, two had lung metastases, one had a right pubic metastasis, one had lung and adrenal metastases, and one had no new metastasis.

Table 1 summarizes the clinical information, including patient age, sex, the location of the tumor, clinical presentation, and laboratory parameters, as well as the clinical follow-up.

Morphological features

Fourteen lesions were located in the extremities, including the proximal femur (six cases), proximal humerus (four

Table 1: Clinical findings in 18 patients with osseous metastases of ccRCC.

Patient no./ sex/age, y	Tumor location	PT, s	PTA, %	ALB/GLO (1.2–2.4)	PLT ($T10^9$/L)	FIB, g/L	Follow-up, month	Interval between nephrectomy and osseous Metastasist, month	Other metastatic lesions	Main symptom
1/M/62	Diaphysis	13.6	94	1.18	330	4.71	7	36	Axial skeleton	Fracture
2/M/62	Proximal femur	13.6	97	1.03	365	2.74	12	1	Axial skeleton	Pain
3/M/49	Proximal femur	13.8	93	1.75	203	2.67	18	0	Axial skeleton	Pain
4/M/63	Proximal humerus	13.6	95	1.42	157	2.31	6	0.5	Axial skeleton	Fracture
5/M/74	Proximal femur	13.1	101.1	1.32	216	3.19	24	120	No	Pain
6/F/64	Proximal radius	14	88	1.47	256	2.85	16	60	Brain	Fracture
7/M/64	Distal femur	14	89	1.38	272	4.11	20	36	Lung	Pain
8/M/64	Proximal femur	12.6	114.0	1.38	268	2.86	10	0	Axial skeleton	Pain
9/M/60	Diaphysis	12.1	126	1.46	278	7.3	15	0	Axial skeleton	Pain
10/M/63	Proximal humerus	12.6	109	1.38	259	5.75	10	0	Axial skeleton	Fracture
11/F/61	Proximal humerus	14.8	79	1.79	198	2.38	12	1.5	Axial skeleton	Pain
12/F/63	Proximal femur	13.6	94	1.65	332	4.71	3	0	Adrenal gland, lung	Fracture
13/M/64	Distal femur	13.8	102	1.54	284	274	10	0	Axial skeleton	Pain
14/M/60	Proximal radius	13.4	98	1.48	299	3.54	9	12	Lung	Fracture
15/M/58	Diaphysis	13.4	103	1.46	304	3.12	20	0	Axial skeleton	Pain
16/M/70	Proximal humerus	13.6	97	1.38	314	2.74	6	36	Brain	Fracture
17/M/70	Diaphysis	13.1	93	1.76	310	2.68	18	0	Pubis	Pain
18/M/70	Proximal femur	12.7	94	1.64	286	2.13	12	36	Axial skeleton	Fracture

PT, plasma prothrombin time; normal range 11.5–14.5 s. PTA, plasma prothrombin time activity; normal range 75–125 %. ALB, albumin; GLO, globulin; normal range 1.2–2.4 g/L. PLT, platelet count; normal range 125–350 $\times$ 10^9/L. FIB, fibrinogen; normal range 2–4 g/L.

cases), distal femur (two cases), and the proximal radius (two cases). Four lesions were located in the diaphysis, including the femur (two cases) and the humerus (two cases). The maximum height of the lesions ranged from 33 to 134 mm (median, 72.1 mm), and the maximum width ranged from 20 to 95 mm (median, 43.3 mm). The height-to-width ratio of the lesions ranged from 1.11 to 3.41, with an average ratio of 1.84 (Table 2). Thirteen lesions had ill-defined margins, and five had well-defined margins. All lesions showed osteolytic destruction, and 16 lesions demonstrated expansile destruction. The cortical bones were interrupted in 15 lesions and were continuous in the other three lesions (Figure 1). Of the 15 lesions, five metastases had obvious pathological fractures. There was no periosteal reaction in any lesion. Fourteen lesions demonstrated irregularly shaped soft tissue masses, and the other four lesions were confined to the marrow cavity without a soft tissue mass.

MRI characteristics

The MR characteristics of 13 lesions are shown in Table 3. Eight lesions demonstrated soft tissue masses with a lobular shape, and the other four lesions were without a soft tissue mass. Eleven cases demonstrated slight hypointensity or isointensity on T1WI and mixed isointensity and hyperintensity on T2WI. In these cases, seven lesions demonstrated soap bubble signs and hypointense separation on T2WI (Figure 2). Two cases demonstrated homogeneous isointense signals on T1WI and slightly hyperintense signals on T2WI. The flow-void sign was observed in six lesions (Figure 1). Seven patients underwent enhanced scanning, and the lesions demonstrated marked marginal enhancement (enhanced similar to normal vessels) with no enhancement in the center (Figure 3).

Table 2: The maximum height, width (mm), and height-to-width ratio of bone metastases of RCC.

	1	2	3	4	5	6	7	8	9	10	11	12	13	14	15	16	17	18
Maximum height	48	90	74	86	59	59	134	60	109	119	49	48	57	33	93	77	57	45
Maximum width	38	75	45	59	29	50	60	26	32	95	44	26	46	20	58	27	24	22
Height-to-width ratio	1.26	1.15	1.64	2.03	2.03	1.18	2.23	2.31	3.41	1.25	1.11	1.85	1.24	1.65	1.60	2.85	2.37	2.04

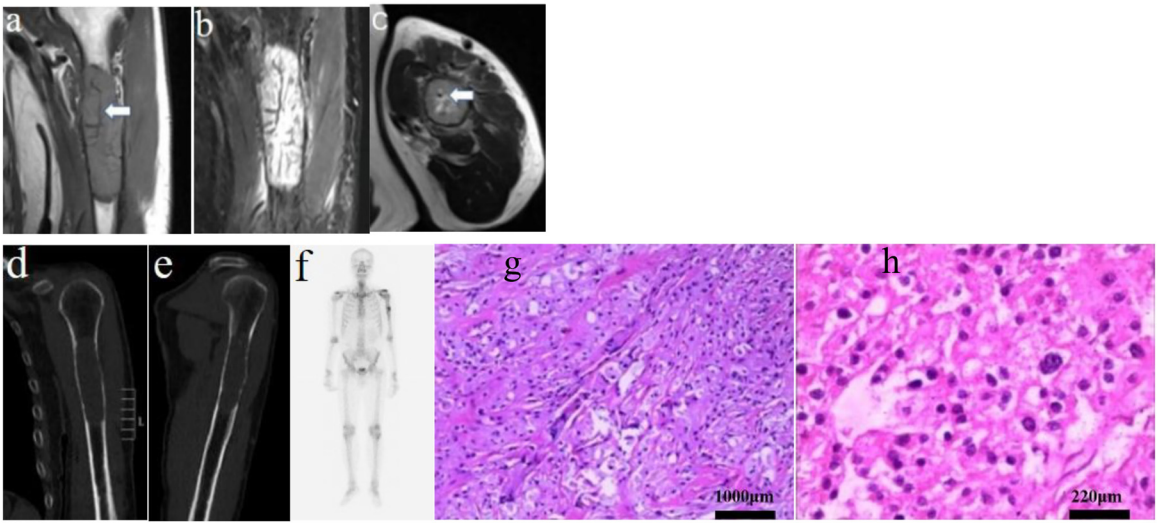

Figure 1: A 64-year-old man with osseous metastasis of ccRCC in his left humerus. (A–C) Coronal T1WI, coronal fat suppression T2WI, and axial T2WI show a mass in the proximal humerus with hypointense tubular structures (arrows). (D–E) Coronal and sagittal CT images show an osteolytic lesion in the bone marrow cavity. (F) Whole-body bone scan shows increased focal uptake in the left humerus. (G–H) The core biopsy sample shows patchy, mildly atypical clear eosinophilic epithelioid tissue within the bone tissue (G, original magnification, ×10; hematoxylin-eosin [H-E] stain) (H, original magnification, ×40; H-E stain).

Table 3: MR signal characteristics of bone metastases of ccRCC.

	1	2	3	4	5	6	7	8	9	10	11	12	13
T1WI													
Signal intensity	Iso-	Hypo-	Iso-	Iso-	Iso-	Hypo-	Hypo-	Hypo-	Hypo-	Hypo-	Hypo-	Iso-	Hypo-
Uniformity	+	–	+	+	+	–	+	–	+	–	–	+	–
T2WI													
Signal intensity	Hyper-	Hyper-	Hyper-	Hyper-	Hyper-	Hyper-	Hyper-	Hyper-	Hyper-	Hyper-	Hyper-	Hyper-	Hyper-
Uniformity	+	–	–	+	–	–	–	–	–	–	–	–	–
Soap bubble sign	–	+	+	–	+	+	+	–	–	+	–	+	–
Separation	–	+	+	–	+	+	+	+	–	+	–	–	–
Flow-void sign	–	+	+	+	–	–	+	–	–	+	–	+	–
Enhancement													
Amplitude	↑↑		↑↑					↑↑	↑↑	↑↑	↑↑	↑↑	↑↑
Uniformity	–		–					–	–	–	–	–	–

+: yes, –: no, ↑: mildly or moderately enhancement, ↑↑: markedly.

Bone scintigraphy

Three patients underwent bone scintigraphy and demonstrated increased focal uptake in the metastatic margins, while there was no significant local uptake in the central regions. See supplementary Table 4 for the summary of the latest publications on bone metastases from ccRCC.

Discussion

Bone metastasis of RCC is more common in older males and occurs in the axial skeleton and proximal appendicular skeleton. When it occurs in the appendicular skeleton, it is most common in the femur and humerus [8]. Stomeo et al. found that infra-diaphragmatic neoplasms are easily

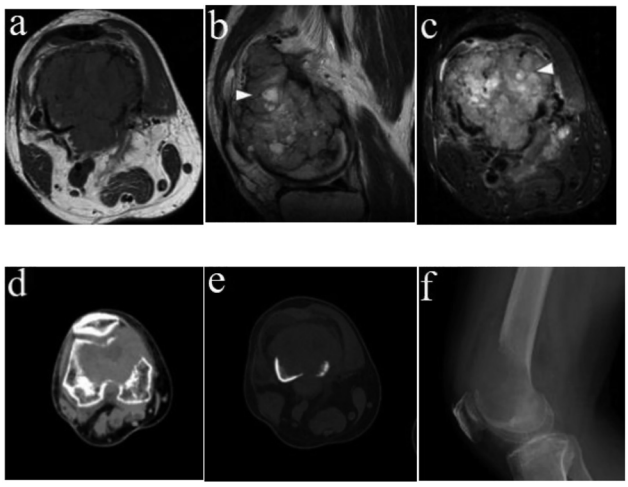

Figure 2: A 62-year-old man with osseous metastasis of ccRCC in his right femur. (A–C) Axial T1WI, sagittal T2WI, and axial fat suppression T2WI show a mass in the distal femur with heterogeneous hyperintensity and a curvilinear area of hypointensity on T2WI (arrowhead). (D–F) CT soft tissue window, CT bone tissue window, and lateral radiograph show an ill-defined osteolytic lesion with expansile change.

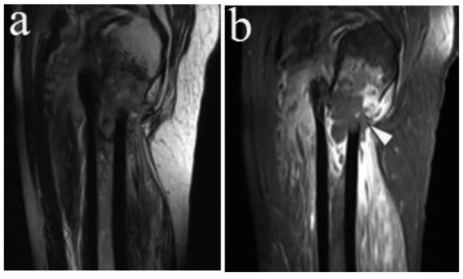

Figure 3: A 63-year-old man with osseous metastasis of ccRCC in his right femur. (A–B) Sagittal T2WI and enhanced T1WI show a mass in the proximal femur with pathological fracture and marked marginal enhancement (arrow).

metastasized to the pelvis in a retrograde manner through the valveless Batson's vertebral venous plexus [16]. Our study results showed that 15 (15/18, 83.3 %) patients were male, with an average age of 63.1 years. This result may be explained by the potential selection bias of retrospective studies, but it also indicated that the bone metastases of RCC were more likely to occur in older men. A study by Choi also reported that 14 (14/16, 87.5 %) patients with RCC bone metastases were older men [6]. In this study, 10 (10/14, 71.4 %) lesions were located in the proximal epiphysis of the appendicular skeleton, with six (6/10, 60 %) lesions in the femur and four (4/10, 40 %) in the humerus, consistent with a previous report [8, 16]. Six patients still had only one bony lesion during the follow-up period. Zekri et al. reported similar results in which 14 (14/31, 45 %) patients had a solitary metastatic lesion from RCC at the time of diagnosis and 8 (8/31, 26 %) patients continued to have only one lesion during the study period [9]. The reason might be that solitary bone metastases of RCC affect the appendicular skeleton more frequently than other solid tumors [9]. Choi et al. reported that RCC frequently manifested first as osseous (often solitary) metastasis from a clinically occult primary tumor [6].

Eight patients were admitted to the hospital due to skeletal-related events (SREs), including four who experienced pathological fractures in long bones. The report by Zekri also demonstrated that pain and pathological fractures were the most frequent SREs of bone metastases, with incidences of 81 and 42 %, respectively, and considered that RCC was a common cause of pathological fractures in long bones [9]. By further comparing the incidence of SREs in metastatic bone disease from RCC and breast cancer, their research demonstrated that the incidence of hypercalcemia was a little higher than that in the latter, but the incidence of pathological long bone fractures and spinal cord compression was similar

Table 4: Summary of the latest publications on bone metastases from ccRCC.

Authors	Year	Primary carcinoma	Number of cases	Results
Zekri [9]	2001	RCC	103	It would therefore be appropriate to evaluate the effectiveness of bisphosphonate treatment for reducing skeletal morbidity in advanced renal cell cancer with bone metastases.
Choi [6]	2003	RCC	20	Observation of the flow-void sign in lesions depicted on MR images may prove helpful for diagnosing osseous metastasis from renal cell carcinoma and for treatment planning.
Setlik [13]	2009	RCC	1	Renal cell carcinoma manifesting as a solitary bone metastasis
Xie [29]	2012	RCC, prostate cancer, lung cancer, breast cancer, melanoma		Unique angiogenic and vasculogenic properties of renal cell carcinoma in a xenograft model of bone metastasis are associated with high levels of vegf-a and decreased ang-1 expression
Pazionis	2014	RCC, thyroid carcinoma	53	Preoperative embolization probably reduces estimated blood loss, particularly for large tumors and during open femoral procedures.
Stomeo [16]	2015			The prognosis of the patients with acrometastases is poor. Special renal cell carcinoma; if treated with radical surgical resection and nephrectomy a better outcome and survival rate shall be expected.

Table 4: (continued)

Authors	Year	Primary carcinoma	Number of cases	Results
Shankar [14]	2016	RCC	1	Renal cell carcinoma with unusual skeletal metastasis to tibia and ankle
Hsieh et al. [3]	2017	RCC		Provide an overview of the biology of RCC, with a focus on ccRCC, as well as updates to complement the current clinical guidelines and an outline of potential future directions for RCC research and therapy
Hellbach [25]	2017	RCC	26	Dual energy CT-based quantification of iodine content of mRCC metastases allows for significantly more sensitive and reproducible detection of anti-angiogenic treatment effects.
Pang [11]	2018	RCC	1	Solitary calvarial haemangioma presenting as metastatic renal cell carcinoma
Murphy [7]	2019	RCC	123	The "flow-void" sign is a common imaging feature within RCC bone metastases.
Chen [23]	2019	Gastric cancer	1	Bone metastases with multiple fluid-fluid levels from gastric cancer
Guillot [27]	2019	RCC	41	The incidence of ONJ was high in this real-life population of patients with mRCC treated with AA therapies combined with dmab.
Xie GanSheng [19]	2019	Prostate cancer	261	Pre-treatment plasma fibrinogen is positively associated with bone metastatic burden in PCa patients. Our results indicate that fibrinogen might be a potential predictor of HVD.
Dong et al. [2]	2020	RCC	168	MSKCC and IMDC criteria may be used for decision making regarding local surgery for patients with BM arising from RCC and for predicting the prognosis.
Migliorini et al. [4]	2020			Update current evidence concerning the aetiogenesis, biological behaviour, and treatment algorithms for painful skeletal metastases.
Beuselinc [8]	2020	RCC	55	WB-DWI/MRI allows better estimation of the prognostic impact of BM in mRCC patients treated with VEGFR-TKIs.
Bian [18]	2020	RCC	187	Validated prognostic model incorporates prothrombin time, prothrombin time, albumin/globulin ratio, platelets, sex and fibrinogen routinely collected from renal cancer patients, identifying subsets of patients with different survival outcomes
Dong [10]	2021	RCC	43,503	The comprehensive predictive tool consisting of nomogram and web calculator contributes to risk stratification which helped clinicians identify high-risk cases and provide personalized treatment options.
Fan [17]	2021	RCC	537	Nomograms were established to predict the risk of BM in RCC and the prognosis of RCC with BM, separately.
Huang [26]	2021	RCC	107	We established an integrative prognosis-related nomogram model incorporating imaging-genomic features and clinical indicators. The IGPF may contribute to a comprehensive prognosis assessment for ccRCC patients.
Ji [5]	2022	RCC	71,414	Developed models can accurately predict the risk and prognosis of kidney cancer with bone metastases and contribute to helping improve decision-making.

[9]. Antczak found that 85 % of the patients with RCC bone metastases experienced SREs at some point in the disease course, but the recent prevalence of SRE-associated hospitalization in patients with RCC bone metastases slightly decreased, with a concomitant reduction in SRE-related in-hospital mortality due to the increased use of imaging and targeted therapies [17]. Thus, imaging examinations play a great role in the discovery of long bone metastases and in preventing the occurrence and development of SREs. Bian et al. reported the predictive value of plasma prothrombin time, plasma prothrombin time activity, albumin/globulin, platelet count, fibrinogen (FIB), and sex for the recurrence-free survival of patients with RCC [18]. In this study, only five patients experienced elevated FIB, of which three (3/5) were accompanied by pathological fractures. The production of plasma fibrinogen typically increases during cancer progression, systemic inflammation, trauma, surgery, and vascular thromboembolism [18]. Xie et al. found a positive correlation between pre-treatment plasma fibrinogen levels and bone metastasis burden in prostate cancer patients [19]. The imaging findings of skeletal lesions, such as dilated metastases and hemorrhagic lesions, especially in patients with bone metastases of unknown origin, can provide valuable clues to primary renal cell carcinoma or thyroid cancer [20]. Early diagnosis and timely treatment can reduce or prevent SREs, alleviate pain, and improve the quality of life, such as preventing impending pathological fractures by assigning scores to the location, nature, size, and pain of bone metastases [20].

The average height-to-width ratio of long bone metastases of RCC was 1.84. The minimum was 1.11, which was greater than 1, indicating that long bone metastases tended to spread along the long bone axis. Toomayan et al. reported that this might be related to the high-resistance natural barriers in the extremities, including cortical bone, articular cartilage, major fibrous septa, tendinous origins, and muscle insertions [21]. Bone metastases of RCC often appeared with the characteristic of typically expansile osteolytic destruction [3]. In this study, only two lesions, which were located in the marrow cavity and had relatively smaller maximum widths of only 23 mm, did not demonstrate expansile bone destruction, so the characteristics of expansile growth were not demonstrated. In the early period, the long bone metastases are small, often located in the marrow cavity, and most are not detected on the X-ray. CT only demonstrates inhomogeneous marrow cavity density and can demonstrate bone marrow metastases before bone destruction occurs [8]. In this group, no lesion demonstrated normal X-rays or abnormal marrow cavity density in CT, which might be related to the larger lesions confirmed by pathological surgical biopsy.

MRI is highly sensitive for detecting bone metastasis as it has the capability to demonstrate intramedullary metastasis, which usually demonstrates T1 hypointensity and T2 hyperintensity [5, 8]. In these cases, three lesions were confined to the marrow cavity and demonstrated mixed signals on T2WI, which were different from the above. The reason could be that the maximum height of the lesion was relatively long, and the lesion could be biopsied by surgical pathology. ccRCC is the most common histologic subtype and accounts for 70 % of RCC. It may exhibit a variety of histoarchitectural patterns, including solid, alveolar, and acinar forms. In addition, ccRCC is highly vascular and can develop a network of small thin-walled sinusoid-like blood vessels. Previous studies reported that when the mass was large, the central areas of hemorrhage, necrosis, and cystic changes resulted in a typically heterogeneous appearance on MR images [3, 22]. In these cases, 10 lesions had heterogeneous hyperintensity on T2WI and fat-suppressed T2WI, and seven lesions demonstrated soap bubble or honeycomb hyperintensity on T2WI surrounded by curvilinear hypointense separation. Chen mentioned similar multiple fluid-fluid levels in gastric cancer bone metastases, which were considered to be due to hemorrhage in the tumors and may be found in any form of highly vascular bone neoplasm [23]. However, the cases in our study only demonstrated soap bubble hyperintensity, which may imply the hemorrhage in the tumor. The linear hypointense separation in the tumor was not a bony component and might have been a network of small thin-walled sinusoid-like blood vessels or a fibrous separation similar to giant cell tumors [6, 24]. Soap bubble hyperintensity and linear hypointense separation could be helpful in diagnosing long bone metastases of ccRCC.

In this study, in addition to the above, six lesions appeared as flow voids with a ccRCC pathological type. Choi reported a similar sign and named it the flow-void sign [6]. Setlik also reported a case of ccRCC bone metastases with prominent flow voids in the lesion and thought it might be related to the unique angiogenesis of ccRCC and its metastasis [13]. Xie et al. developed a xenograft model to study the unique angiogenic characteristics of bone metastases of RCC [25]. Compared to lung cancer, breast cancer, RCC, prostate cancer, and melanoma, ccRCC itself is more likely to promote the formation of tumor blood vessels due to its significant expression of vascular endothelial growth factor. The number, diameter, and density of blood vessels in the lesions and metastases are several times higher than those of other tumors [25]. Therefore, ccRCC and its metastases are hypervascular and prone to exhibiting flow void signs [26]. Pang reported a case of skull metastases of ccRCC with an initial diagnosis of hemangioma [11]. Therefore, improving the understanding of the flow-void sign is helpful for the diagnosis and clinical treatment of bone metastasis of ccRCC, including anti-angiogenic therapies and immunotherapy [6, 27]. The presence of the flow-void sign on MRI should raise the suspicion of RCC bone metastasis. When considering biopsy or other interventions for lesions, the flow-void sign should also be used as an indicator of vascular overgrowth [7]. Pazionis performed a case-control study and found that preoperative embolization reduced estimated blood loss and operative time, particularly for large tumors and during open femoral procedures [28]. Recent studies showed that besides using tumor diameter as a criterion for evaluating treatment effectiveness, measuring the contrast enhancement of ccRCC may be a more relevant tool for providing information on anti-angiogenic treatment responses [29]. Hellbach et al. found that the quantitative analysis of iodine content in ccRCC metastatic lesions based on dual-energy CT could significantly improve the sensitivity and repeatability of anti-angiogenic treatment effects [29].

Besides solitary plasmacytoma, solitary malignant tumors can also represent osteosarcoma, chondrosarcoma, and bone metastasis from lung cancer in the long bone, which should be differentiated from a solitary LBM of RCC. Long bone solitary plasmacytoma has been described as single punched-out osteolytic lesions, diffuse osteopenia, fractures, and rarely, osteosclerosis. The lesion demonstrates isointensity on T1WI and hyperintensity on T2WI and might form a “mini-brain” appearance on MR. The mini-brain appearance results from localized bony destruction with the formation of thickened trabeculae, which are arranged in a peripheral radial pattern simulating sulci within the brain [30]. The soft tissue mass is more uniformly enhanced. Bone scans obtained with 99 mTc

have resulted in an underappreciation of the extent of the disease [31]. Primary osteosarcoma in the elderly often occurs in the distal femur and proximal humerus, with mainly characteristic appearances of irregular bone destruction, obvious periosteal reaction, sometimes Codman's triangle, and a mineralized soft-tissue mass. The sensitivity of MR for identifying tumor bone matrix is poor, and the combination of X-ray and CT is needed to better identify it [31]. Chondrosarcoma is often located in the metaphysis of the long bone, showing expansile destruction, deep endosteal scalloping, and a classical lobular appearance [32]. The pattern of cartilaginous matrix calcification in the mass might be punctate, flocculent, or typical ring-and-arc-type [32]. The lesion demonstrates hypointensity on T1WI and heterogeneous hyperintensity on T2WI with areas of obvious hyperintensity and peripheral and septal enhancement. Sometimes this type of lesion shows rings or amorphous enhanced nodules in the mass [32]. Solitary long bone metastasis from lung cancer could also show expansile changes and little soap bubble hyperintensity on T2WI [33]. Distinctions between the two cases still need further study.

This retrospective study had several limitations. First, it had a small sample size because of the low incidence of LBM. However, in our experience, the expansile osteolytic destruction, soap bubble hyperintensity, the flow-void sign, and other signal characteristics seemed to be typical of LBM of RCC. Second, due to its retrospective analytic nature and pathologically confirmed metastatic lesions, selection bias was inherent as bone metastases may have more complex or atypical manifestations. The patients in this report were a selected population, i.e., patients with clear cell renal carcinoma, and we did not collect other pathological types of renal cell carcinoma. We hope to share our results, which will be helpful in diagnosing this disease, but they must also be verified in further studies using a larger sample size.

LBM of RCC was common in older men and occurred in the proximal femur and humerus. The lesions tended to spread along the long bone axis, with mostly expansile osteolytic destruction, soap bubble or honeycomb hyperintensity, and linear hypointense separation. Also, the flow-void sign might be present in ccRCC metastasis. The above characteristics could be useful for diagnosing LBM of RCC.

Research funding: The author(s) received no specific funding for this study.

Author contributions: Data collation, Z.R., S.D.B; Literature and clinical research, S.D.B.; Manuscript – original draft, S.D.B.; Manuscript – review and editing, Z.R.; Approval of the submitted version of the manuscript, all authors.

Conflicts of interest: The authors declare that they have no conflicts of interest to report regarding the present study.

Availability of data and materials: The raw data may be made available upon reasonable request from the corresponding author.

Consent for publication: Written informed consent was obtained from the patient for the publication of this case report and accompanying images.

Ethics approval and consent to participate: Informed written consent has been obtained from the patients in this case report to publish this paper. The present study involved human participants, and it was conducted considering ethical responsibilities according to the World Medical Association and the Declaration of Helsinki.

References

1. Chen W, Zheng R, Baade PD, Zhang S, Zeng H, Bray F, et al. Cancer statistics in China, 2015. CA Cancer J Clin 2016;66:115–32.
2. Dong Y, Wang Z, Lu X, Wu Z, Zhang Z, Yu Y, et al. Clinical outcomes of 168 Chinese patients after local surgery for bone metastases arising from advanced renal cell carcinoma. Cancer 2020;126:2079–85.
3. Hsieh JJ, Purdue MP, Signoretti S, Swanton C, Albiges L, Schmidinger M, et al. Renal cell carcinoma. Nat Rev Dis Prim 2017;3:17009.
4. Migliorini F, Maffulli N, Trivellas A, Eschweiler J, Tingart M, Driessen A. Bone metastases: a comprehensive review of the literature. Mol Biol Rep 2020;47:6337–45.
5. Ji L, Zhang W, Huang J, Tian J, Zhong X, Luo J, et al. Bone metastasis risk and prognosis assessment models for kidney cancer based on machine learning. Front Public Health 2022;10:1015952.
6. Choi JA, Lee KH, Jun WS, Kang HS. Osseous metastasis from renal cell carcinoma: "flow-void" sign at MR imaging. Radiology.2003;228:629–34
7. Murphy J, Patel A, James SL, Botchu R, Davies AM. "Flow-void" sign in osseous metastatic renal cell carcinoma. Clin Radiol 2019;74:111–5.
8. Beuselinck B, Pans S, Bielen J, De Wever L, Noppe N, Vanderschueren G, et al. Whole-body diffusion-weighted magnetic resonance imaging for the detection of bone metastases and their prognostic impact in metastatic renal cell carcinoma patients treated with angiogenesis inhibitors. Acta Oncol 2020;59:818–24.
9. Zekri J, Ahmed N, Coleman RE, Hancock BW. The skeletal metastatic complications of renal cell carcinoma.Int J Oncol.2001;19:379–82.
10. Dong S, Yang H, Tang ZR, Ke Y, Wang H, Li W, et al. Development and validation of a predictive model to evaluate the risk of bone metastasis in kidney cancer. Front Oncol 2021;11:731905.
11. Pang C, Loo YL, Corns R, Mohammed R. Solitary calvarial haemangioma presenting as metastatic renal cell carcinoma. BMJ Case Rep 2018;2018: bcr2017223334.
12. Kong Y, Wang J, Li H, Guo P, Xu JF, Feng HL. Pathological clavicular fracture as first presentation of renal cell carcinoma: a case report and literature review. Cancer Biol Med 2015;12:409–12.
13. Setlik DE, McCluskey KM, McDavit JA. Best cases from the AFIP: renal cell carcinoma manifesting as a solitary bone metastasis. Radiographics 2009;29:2184–9.
14. Shankar K, Kumar D, Kumar KV, Premlata C. Renal cell carcinoma with unusual skeletal metastasis to tibia and ankle: a case report and review of literature. J Clin Diagn Res 2016;10:XD01–2.
15. Vaishya R, Vijay V, Vaish A. Bilateral acrometastasis in a case renal cell carcinoma. BMJ Case Rep 2014;2014:bcr2014206402.

16. Stomeo D, Tulli A, Ziranu A, Perisano C, De Santis V, Maccauro G. Acrometastasis: a literature review. Eur Rev Med Pharmacol Sci 2015; 19:2906–15.
17. Fan Z, Huang Z, Huang X. Bone metastasis in renal cell carcinoma patients: risk and prognostic factors and nomograms. JAMA Oncol 2021;2021:5575295–17.
18. Bian Z, Meng J, Niu Q, Jin X, Wang J, Feng X, et al. Prognostic role of prothrombin time activity, prothrombin time, albumin/ globulin ratio, platelets, sex, and fibrinogen in predicting recurrence-free survival time of renal cancer. Cancer Manag Res 2020;12:8481–90.
19. Xie GS, Li G, Li Y, Pu JX, Huang YH, Li JH, et al. Clinical association between pre-treatment levels of plasma fibrinogen and bone metastatic burden in newly diagnosed prostate cancer patients. Chinese Med J 2019;132:2684–9.
20. Umer M, Mohib Y, Atif M, Nazim M. Skeletal metastasis in renal cell carcinoma: a review. Ann Med Surg 2018;27:9–16.
21. Toomayan GA, Robertson F, Major NM. Lower extremity compartmental anatomy: clinical relevance to radiologists. Skeletal Radiol 2005;34:307–13.
22. Alshenawy HAS. Immunohistochemical panel for differentiating renal cell carcinoma with clear and papillary features. Pathol Oncol Res 2015; 21:893–9.
23. Chen M, Yuan H. Bone metastases with multiple fluid-fluid levels from gastric cancer: a case report and review of literature. Skeletal Radiol 2019;48:813–7.
24. Çomunoğlu N, Kepil N, Dervişoğlu S. Histopathology of giant cell tumors of the bone: with special emphasis on fibrohistiocytic and aneurysmal bone cyst like components. Acta Orthop Traumatol Turcica 2019;53:35–9.
25. Hellbach K, Sterzik A, Sommer W, Karpitschka M, Hummel N, Casuscelli J, et al. Dual energy CT allows for improved characterization of response to antiangiogenic treatment in patients with metastatic renal cell cancer. Eur Radiol 2017;27:2532–7.
26. Huang Y, Zeng H, Chen L, Luo Y, Ma X, Zhao Y. Exploration of an integrative prognostic model of radiogenomics features with underlying gene expression patterns in clear cell renal cell carcinoma. Front Oncol 2021;11:640881.
27. Guillot A, Joly C, Barthélémy P, Meriaux E, Negrier S, Pouessel D, et al. Denosumab toxicity when combined with anti-angiogenic therapies on patients with metastatic renal cell carcinoma: a GETUG study. Clin Genitourin Cancer 2019;17:e38–43.
28. Pazionis TJ, Papanastassiou ID, Maybody M, Healey JH. Embolization of hypervascular bone metastases reduces intraoperative blood loss: a case-control study. Clin Orthop Relat Res 2014;472:3179–87.
29. Xie C, Schwarz EM, Sampson ER, Dhillon RS, Li D, O'Keefe RJ, et al. Unique angiogenic and vasculogenic properties of renal cell carcinoma in a xenograft model of bone metastasis are associated with high levels of vegf-a and decreased ang-1 expression. J Orthop Res 2012;30:325–33.
30. Zhang D, Andrade JP, Cassis J, Soares P. The "mini brain" sign in a case of vertebral hemangioma mimicking solitary plasmacytoma of the spine: refutal of a pathognomonic sign? Clin Neuroradiol 2020;30:173–5.
31. Kumar R, Kumar M, Malhotra K, Patel S. Primary osteosarcoma in the elderly revisited: current concepts in diagnosis and treatment.Curr Oncol Rep.2018;20:13
32. Ghafoor S, Hameed MR, Tap WD, Hwang S. Mesenchymal chondrosarcoma: imaging features and clinical findings. Skeletal Radiol 2021;50:333–41.
33. Basu Mallick A, Chawla SP. Giant cell tumor of bone: an update. Curr Oncol Rep 2021;23:51.